INFRAMATION

Use of Thermography to Calibrate Fusion Welding Procedures in Virtual Fabrication Applications

Duncan Camilleri, Tom Gray, Tugrul Comlekci
Department of Mechanical Engineering, University of Strathclyde

ABSTRACT

The application of infrared thermography to the measurement of transient temperature fields generated by fusion welding of ship structures is described. The purpose is to capture real data from practical welding situations, which can then be used as input to computational simulation of welding manufacturing operations (virtual fabrication). Workpiece distortion due to thermal mismatch strains constitutes a major technological and economic problem in welding fabrication, and there is worldwide research interest in simulation techniques that facilitate off-line investigation of methods to reduce distortion in real applications. The effectiveness of such methods depends critically on the thermal input stage, where the complex effects of variable arc energy transfer, non-linear material properties, and workpiece / fixture heat-sink variables are present in a practical case. Thermography provides a unique method to measure such parameters on a whole-field basis.

The paper presents measurement comparisons made on large welded plate structural components between whole-field thermographic data, thermocouple data, finite-element thermal analysis, and analytical approaches. The paper also addresses relevant thermal imagery problems in this context, such as emissivity calibration and compensation methods for lens distortion. Thermography is shown to be an ideal way to identify the outcomes of practical features such as thermal discontinuities in the workpiece and the effects of weld preparation and process variables on the thermal transfer efficiency of the welding process electrical energy.

Keywords: welding, transient temperatures, infrared, thermography, correction factors

INTRODUCTION

Nomenclature

K	Plate thermal conductivity (J/ms °K)	r	Radial distance behind heat source (m)
K_o	Bessel function - second kind, zero order	t	Thickness of plate (m)
T_s	Surface temperature (°K)	v	Welding speed (m/s)
T_a	Ambient temperature (°K)	ε_s	Surface emissivity
T_c	Temperature obtained from camera (°K)	λ	Thermal diffusivity (m²/s)
Q	Heat input rate = efficiency×V×I (W)	N_k	Shape functions
		ϕ	Nodal temperature (°K)

Background

This investigation was carried out in the context of a study to improve the prediction and control of welding distortion in thin plate welded structures. The study is concerned in particular with out-of-plane distortion, which is a major problem in fabrication of ships, bridges, pressure vessels, and similar structures. The transient thermal field that accompanies any fusion welding procedure is the major driver of the distortion process, and this field is difficult to quantify theoretically, especially in a practical application. The work described in this paper shows how thermography can be used uniquely to determine the key thermal information in such situations. This capability, in conjunction with thermo-elasto-plastic theoretical computation, makes it possible to predict out-of-plane distortions that may arise and to determine alternative manufacturing procedures that can reduce such effects.

The modeling approach adopted by the present project is based on a strategy whereby the various parts of the thermo-mechanical problem are uncoupled. That is, the thermal transient, thermo-elasto-plastic, and structural stages of the process are treated separately. The first step is to establish the transient

thermal distributions caused by a given welding process in the geometry of interest. This may be achieved in a variety of theoretical ways, ranging from the early analytical treatments of Rosenthal [1], Rykalin [2], and Wells [3] to the finite element-based methods, as reviewed recently by Lindgren [4], [5].

Two computational strategies, including analytical solutions, for the prediction of welding thermal transients are presented in this study. However, these are of doubtful use without experimental information from actual welding tests. In the first place, the development and verification of the assumptions in the finite element analysis of welding depend on such information. L. E. Lindgren [5] also concludes that uncertain material properties and the problem of predicting the net heat input mean that the success of simulations must depend to a large extent on experimental work. Prediction of thermal transients, whether through thermal finite element analysis or empirical formulas, relies on measured transient temperatures or information from the resultant weld microstructure. In particular, most of the simulations assume an energy transfer efficiency, which is not normally known, unless through comparison with experimental results. This efficiency is used to adjust the total heat input energy that flows into the welded plate. Hence, the use of thermography to determine efficiency, supplemented by thermocouple measurements, makes infrared imagery an essential tool in the final prediction of welding distortions.

Thermography gives an overall thermal picture of the welded plate, as distinct from the point measurements given by thermocouples. Thermography also plays an important role in the investigation of thermal transients in indefinite heat absorption systems, where external heat sinks may be present. It can also determine the thermal pattern for distortion near the ends of plates, where a non-quasi static pattern exists. Thermography has not been widely used in the welding field. Typical reported investigations include that of Cheng et al. [6], Khan et al. [7], and Boillot et al. [8]. Cheng et al. used thermography as a cross reference for the finite element simulations, while Khan et al. and Boillot et al. directed the use of thermography to the control of welding process problems, such as arc misalignments.

The main theme of this paper is that thermography offers the possibility to investigate the thermal transients that trigger welding distortions, without the need for finite element simulations; i.e., the thermal patterns obtained from thermography can provide an input to the decoupled analysis. However, perhaps due to the cumbersome calibration required, including the knowledge of surface emissivity at different temperatures and mapping of specific points under investigation, it has not typically been used in industry for this purpose. The present study also concentrates on providing a mapping strategy via finite element shape functions together with a simplified means of measuring the emissivity.

THERMOGRAPHIC MEASUREMENT AND CALIBRATION TECHNIQUES

The thermographic principle is based on capturing infrared emission from the subject under investigation. The thermographic camera used in the present study, the ThermaCAM® SC 500 from FLIR Systems, captures infrared radiation at wavelengths in the range of 3 to 12 μm. The accuracy of the data obtained depends on the emissivity of the plate, which in turn is highly dependent on the surface condition of the material. Furthermore, emissivity is also a function of temperature, whereby it tends to increase with temperature for metallic materials and conversely decreases with an increase in temperature for non-metals. It should be pointed out that, while grey surfaces radiate a constant fraction of the blackbody radiant energy over the entire spectrum, in real surfaces the emissivity is also a function of the wavelength.
Due to the number of dependent variables, an experiment had to be devised to quantify the emissivity of the specimens under investigation. This was performed within the spectral range of the thermographic infrared camera and at temperatures ranging from 25°C to 500°C. Higher temperatures were not considered, due to the complexity associated with the experimental setup, and because temperatures below 300°C are the main contributing factors to welding distortion. For consistent emissivity, all welded structures in the present study were shot blasted and spray painted with a zinc silicate primer prior to welding. Shot blasting was performed using a steel grit of particle size 0.6–1.0 mm, while the coating was made up of a grey Interplate 937 Nippe Cermao – zinc silicate shop primer, consisting of two parts: ZnO in a silicate binder. The emissivity was measured via a thermocouple array attached at various positions on a heated, shot blasted, primed fin as shown in
Figure 1.

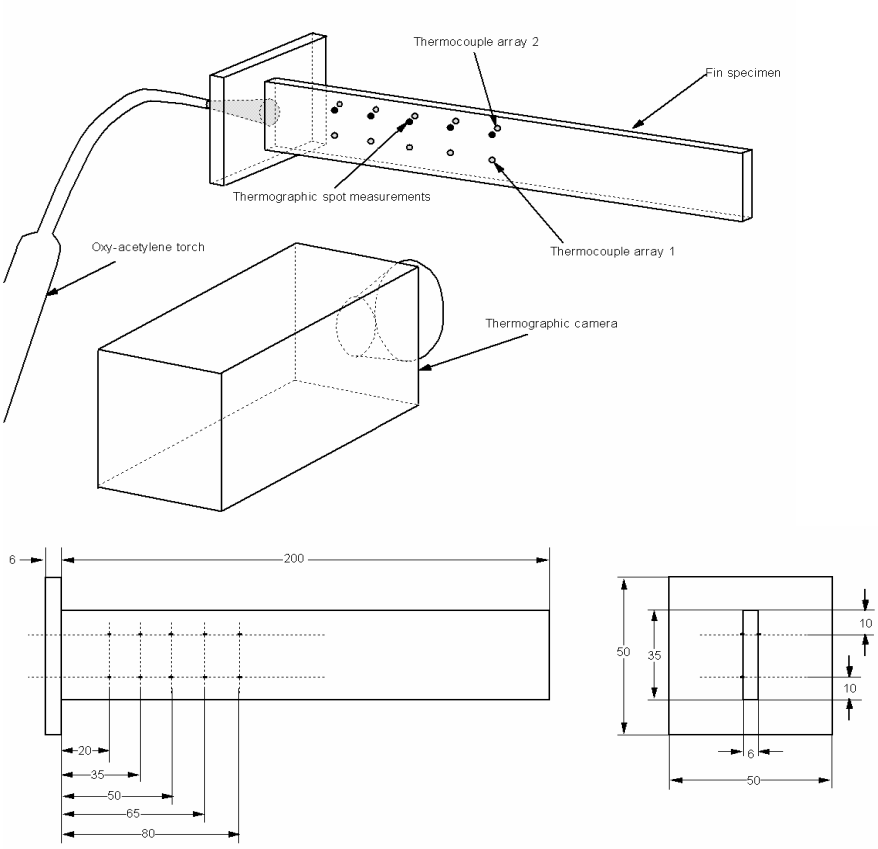

Figure 1. Experimental set-up for the determination of emissivity

Figure 1a shows the experimental set-up, while
Figure 1b shows the positions of the thermocouples and spot points where thermographic readings were recorded. The fin was heated by means of an oxyacetylene torch, until a steady state condition prevailed. Synchronous temperature readings, from the thermocouples and the infrared camera, were taken at various instances during the steady and cooling phase. By assuming symmetry in the temperature profiles, the temperature readings from the thermographic infrared camera at positions shown in Figure 1b would relate to the thermocouple readings. The temperatures indicated by the images, together with the thermocouple readings and the ambient temperature, were used to determine the emissivity at different temperatures, via the relationship given by Equation 1.

$$\varepsilon_s = \frac{T_c^4 - T_a^4}{T_s^4 - T_a^4} \qquad \textit{Equation 1}$$

Readings obtained from 7 experiments were averaged to obtain specific emissivities within different temperature ranges.
Figure 2 shows the emissivity of the primer-coated steel, with respect to the specimen surface temperature.

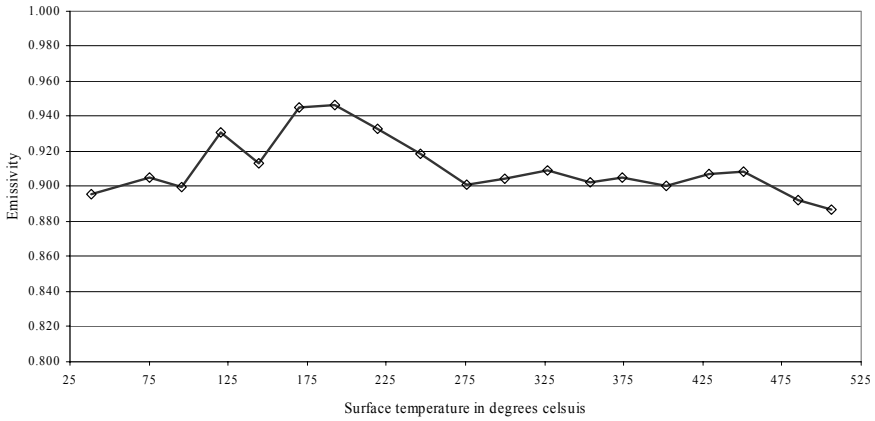

Figure 2. Surface emissivity of zinc silicate shop primer coated steel at various temperatures

An important objective of the thermographic analysis was to relate acquired data to precise positions relative to the welding head. Hence, the welding head and thermographic infrared camera were mounted together in a fixed position. Lens aberrations in this system distort the image, and careful calibration was required to ensure positional accuracy. A transformation matrix was developed, obtained through the shape functions of a four-node linear element. Lens aberrations were particularly evident in the wide-angle lens.

Figure 3a shows the distortion of a rectangular wire mesh when viewed using a 45° lens at a distance of approximately 1 m. The image represents a grid of dimensions 550 mm x 750 mm, the size of each element being 50 mm x 50 mm. The contrast between the background temperature and the grid was achieved by means of electrically heated nickel chrome wire, equally spaced at fixed distances.
Based on the known grid / element dimensions, shown in
Figure 3a, a transformation matrix was obtained to relate a point in a second coordinate system defining the region of interest to the pixel position. Hence, the temperature at certain points from a specified local coordinate, taken to be the origin of the plate under investigation, could be found, while taking into consideration any effects resulting from changes in emissivity.

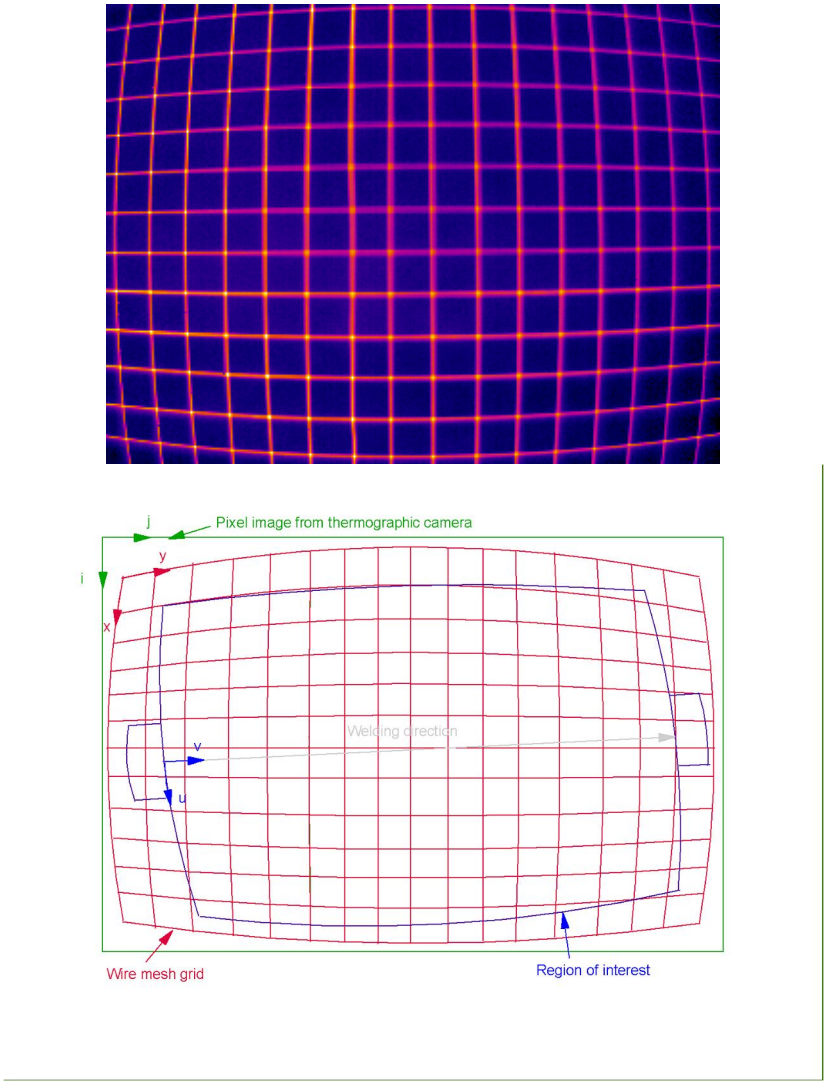

Figure 3. a. Distorted image corresponding to a rectangular wire mesh; b. Coordinate transformations for the mapping of points defined in the region of interest

Figure 3b shows the coordinate transformations performed for the mapping of points specified in the region of interest with coordinate axis u-v. The program performs the transformation from the i-j to the x-y and finally to the u-v coordinate systems and consists of a number of subroutines, integrated in the main program shown in
Figure 4.

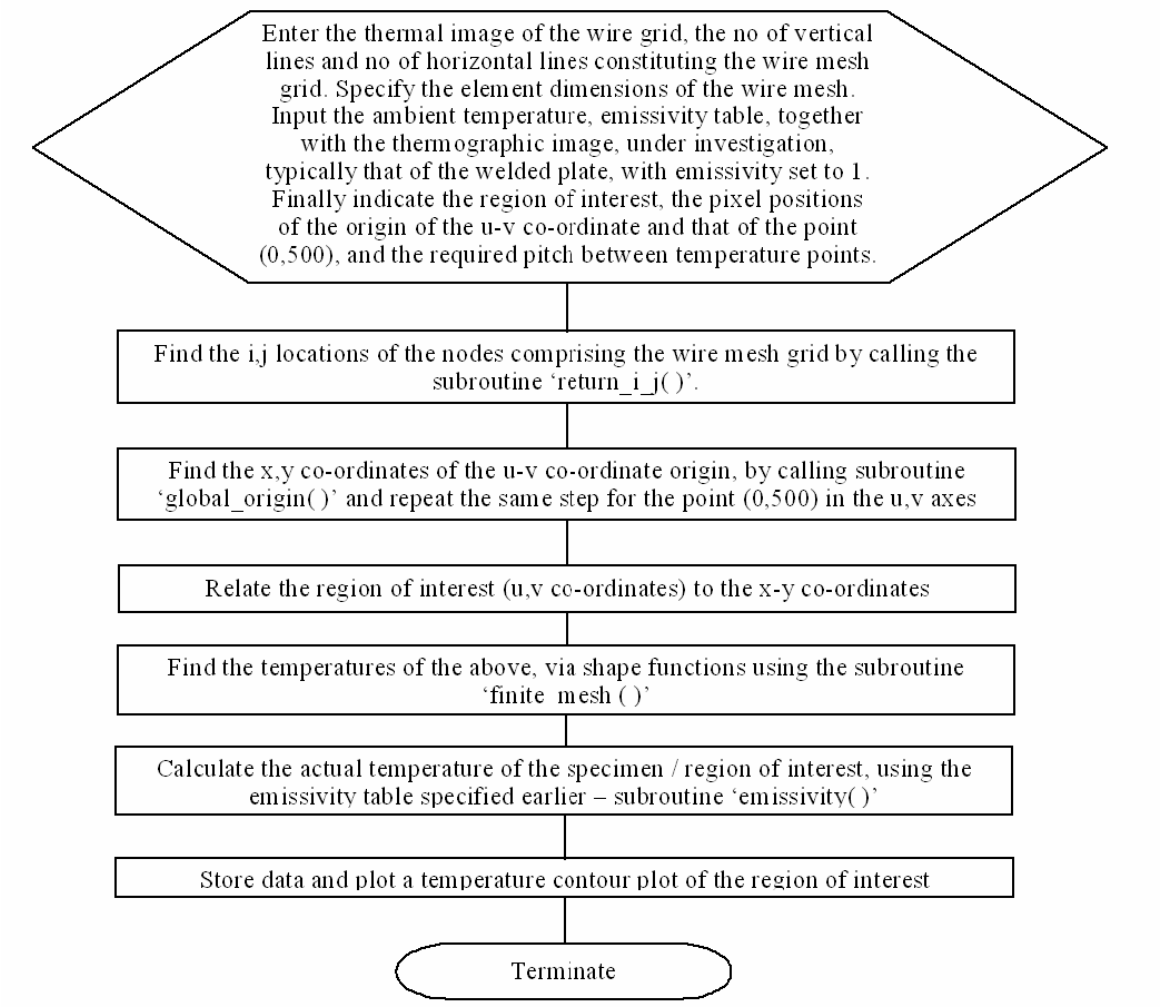

Figure 4. Pseudo-code of the main program

The prime objective of the program is to find the pixel positions of wire mesh nodes, i.e., the intersection of the heated wires. This subroutine is named 'return_i_j()' and is based on the fact that at the intersection of the heated wires a higher temperature prevails. Each nodal position in the wire mesh grid is assigned 5 values that include the i, j, x, and y locations relative to their respective coordinates and the temperature ϕ obtained from the thermographic image of the welded plate. The subsequent sub-program transforms the i-j values of the origin and angular orientation of the u-v coordinate system to the x-y coordinate system, via an inverse transformation of the shape functions given in
Figure 5: 'global_origin()'. Using this information, the subsequent subroutine 'finite_mesh()' returns a flat, undistorted array of the thermal pattern defining the region of interest. The transformation from the u-v coordinate axis to the x-y coordinate axis is simply an orientation conversion. It is assumed that both coordinates lie in the same plane. On the other hand, the transformation from the x-y to the i-j coordinates makes use of the linear Lagrangian four-node shape functions listed in
Figure 5. The program finds the pixel i-j values of the points of interest, specified within the region of consideration, and returns the temperatures at those points. Finally, the program uses another subroutine, 'emissivity()', that finds the actual temperature of the specimen by taking into account the emissivity quantified in
Figure 2.

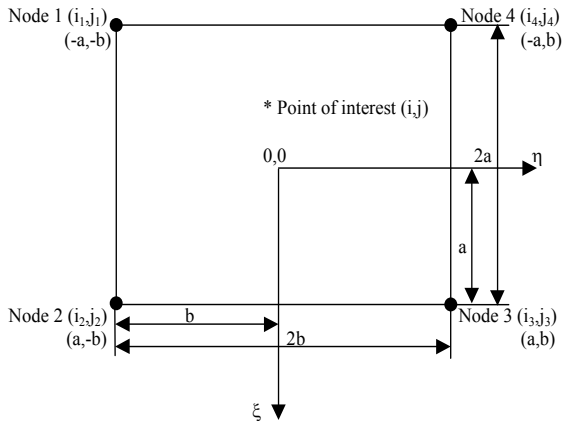

$$N_1 = \frac{(a-\xi)(b-\eta)}{4ab} \qquad N_4 = \frac{(a-\xi)(b+\eta)}{4ab}$$

$$N_2 = \frac{(a+\xi)(b-\eta)}{4ab} \qquad N_3 = \frac{(a+\xi)(b+\eta)}{4ab}$$

$$\phi = \sum_{k=1}^{4} N_k \phi_k \qquad \phi = f(i,j)$$

Figure 5. Shape functions of a four node linear Lagrangian type element

Assuming that the primer is opaque to infrared radiation, and hence the absorptivity is equal to the emissivity, and that the background radiation is assumed to be coming from a black body, the final surface temperature is given by Equation 2.

$$T_s = \left(\frac{1}{\varepsilon_s} \cdot \left[T_c^4 - T_a^4 \right] - T_a^4 \right)^{1/4} \qquad \textit{Equation 2}$$

The mapping algorithm was tested out by butt welding 500 mm square x 6 mm thick CMn steel plates to S355K2G3 (BS4360 Grade 50D), using an automatic, flux-cored 20% CO2, 80% Ar shielded process. The nominal heat input rate was 1.14–1.24 kJ/mm, corresponding to 23V, 250A, and 4.8mm/s travel speed. A typical contour is shown in Figure 6a, obtained from the thermographic infrared camera, and Figure 6b shows the contour plot after the calibration and lens distortion correction factors were incorporated.

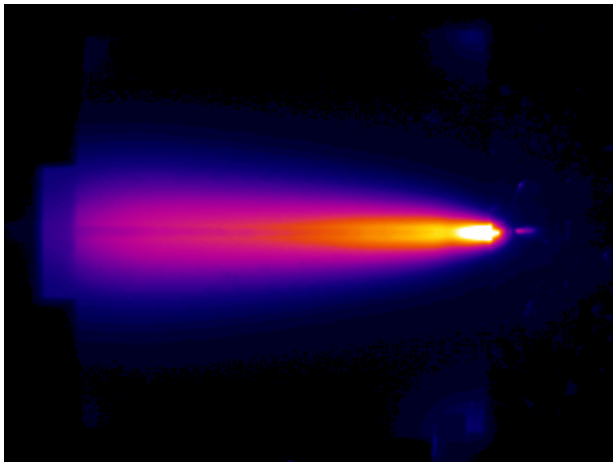

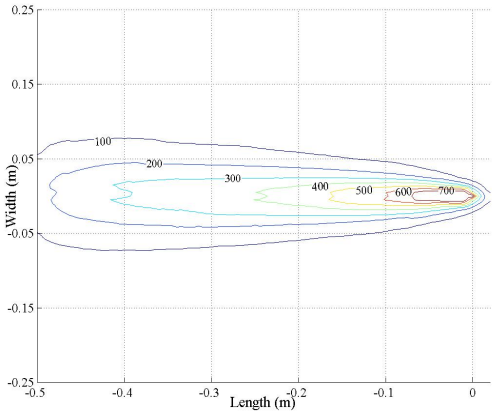

Figure 6. Temperature contour plot near end of weld run

THEORETICAL INVESTIGATION

Thermal welding transients depend highly on the net heat input and the material properties, the latter being non-linearly dependent on temperature. In the case of the heat input, thermocouple readings were used as a cross reference to find the efficiency of the welding process. That is, the thermal efficiency value, used in the theory to convert welding electrical energy into heat input, was adjusted to match the temperature profiles of the computations to the thermocouple data profiles at the specific locations. The strategies presented here include simplified approaches together with a full three-dimensional analysis of the problem.

SIMPLIFIED ANALYTICAL SOLUTION

Prior to the development of computer technology, attempts to quantify thermal transients in welding were purely analytical. A number of simplifications and assumptions were made. The thermal properties of the base material were assumed to be constant and independent of temperature. Further simplification to the problem was made by assuming that the heat sources move at a constant speed, such that the temperature profile, relative to the heat source position, is quasi-stationary. The most significant early determinations were provided by Rosenthal [1] and Rykalin [2], where appropriate solutions for linear, two-, and three-dimensional heat flows in solids of infinite size were derived. The well-known two-dimensional heat conduction equation, given below, is applicable to the case under consideration.

$$T_s - T_a = \frac{Q}{2\pi Kt} e^{\frac{-vx}{2\lambda}} K_o\left(\frac{vr}{2\lambda}\right) \qquad \textit{Equation 3}$$

Though the solution converges to an unrealistic infinite temperature at the weld pool center, it provides satisfactory information at the far field, provided that the correct energy efficiency and thermal properties are used. The thermal plot, shown in
Figure 7, was generated using Equation 3, assuming an efficiency of 0.825, an averaged specific heat of 782.6 J/kg°C, and an average conductivity of 69.58 J/ms°C.

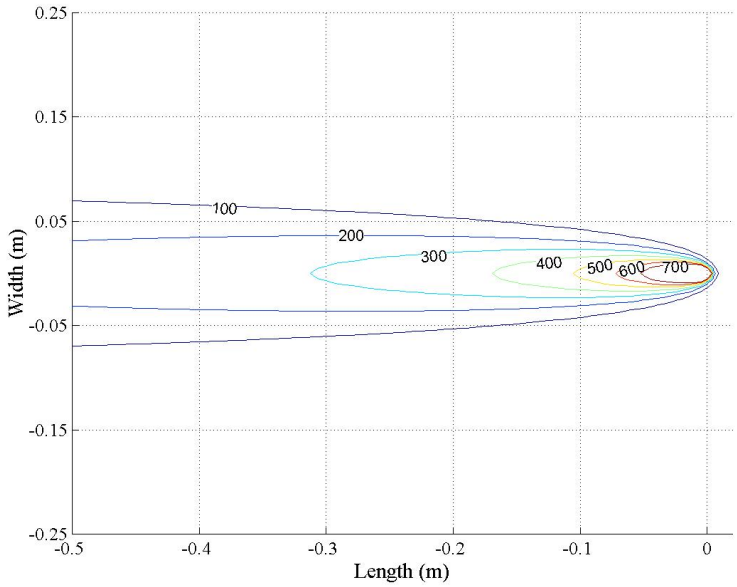

Figure 7. Two-dimensional analytical solution – 0.825 efficiency

Comparison of the thermal plots in Figures 7 and 6 shows that the trailing edge of the plate in the experiment has not reached steady state, as indicated by 100°C and 200°C isotherms, from the thermographic contour plot.

COMPUTATIONAL FINITE ELEMENT MODEL

Various strategies are possible in this aspect, ranging from full a two-dimensional cross-section to full three-dimensional transient models. Finite element analysis provides the useful possibility to define non-linear, temperature-dependent material properties and boundary conditions. Typically, specific heat and conductivity are the prime properties whereby effects such as latent heat and phase transformation can be taken into account, albeit that the material properties are known. Furthermore, heat loss effects due to radiation and convection were modeled in the computational analyses by defining non-linear, temperature-dependent film coefficients for the top and bottom surfaces of the plates. A comparison between the various thermal computation strategies is given in [9], where it is concluded that a three-dimensional transient model provides the most accurate analysis, although it lacks computational

efficiency. In this analysis, the simulated heat source is moved at constant velocity along the weld line in a series of fine 'load' steps. Various ways of simulating weld deposition and energy input were explored. In the first instance, the weld fusion zone was assumed to be present from the beginning, ignoring the effects of undeposited weld ahead of the welding arc. On the other hand, the element 'birth and death' technique was applied to the weld zone to simulate the transition in thermal capacity between the empty groove and filled weld. In both cases, the process energy was defined alternatively by means of a volumetric heat input applied to the fusion zone and by means of a nominal distribution heat flux applied to the surface of the plate after the work of Friedman [10].

The resulting differences between the different heat input modeling approaches were not major. On the other hand, the 'birth and death' element approach resulted in higher temperature when the same welding efficiency of 0.825 was used. This relates to the fact that less material was available to absorb the heat. Thus, the effectiveness of the computational approaches depends highly on the weld efficiency assumed.

Figure 8 shows the thermal contour plot at the end of the weld run. As opposed to the simplified analytical approaches, the contours follow the thermographic results more closely.

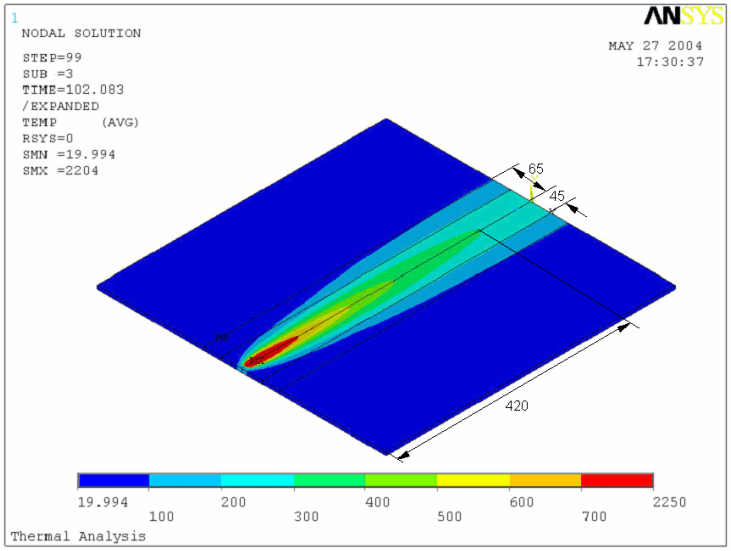

Figure 8. Thermal contour plot from three-dimensional finite element model

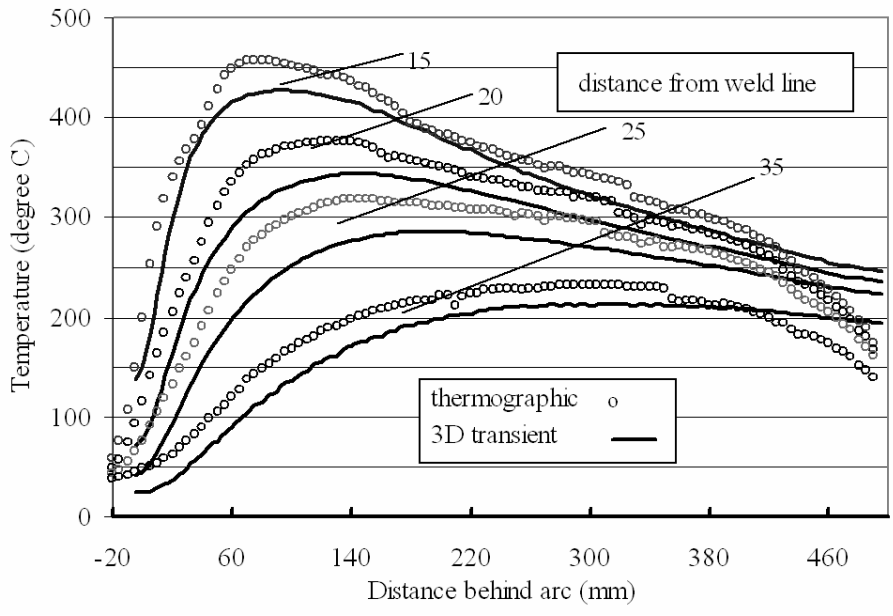

Figure 9. Comparison between 3D results and thermographic data at specific distances from weld axis

The difference between the finite element results and the thermographic data is more apparent at the trailing edge of the plate, as shown in Figure 9 at distances greater than 420 mm. It is evident that the thermal sinks due to the run-off tabs are not present, particularly because the run-off plates were not modeled and because of the unknown thermal heat transfer occurring between the plate and tabs. Furthermore, the thermographic results show an offset in temperature due to the radiation effect from the arc. The data shows that thermography is an effective tool in the measurement of thermal transients, particularly in defining non-quasi static thermal transients.

DISCUSSION

Comparison of the various theoretical and experimental plots of transient temperature in sample plates (Figures 6-9) shows that whole-field imaging is essential to reveal significant features of the thermal conditions that cannot be modeled theoretically in a practical sense. Thermographic imaging fulfills this task admirably, and it would be difficult to visualize a more effective tool. The sample plates represented a relatively straightforward case, where the welding process was well characterized, and the plate was supported in a manner that simplified the prediction of thermal losses. Thermography would, therefore, be even more valuable in other more complex practical cases, where ideal boundary conditions would not be achievable. The authors have also applied thermography to other cases involving fillet welding of stiffeners and the addition of heat sink materials to control temperature distributions. These applications will be the subject of later publications.

Interpretation of thermal images in the context of distortion prediction is beyond the scope of this paper, but is it covered in references [11] and [12]. These references show that the key parameters relevant to the prediction of longitudinal contraction force, which is the main driver for out-of-plane and buckling distortions, are the maximum temperatures reached at transverse locations on a transverse slice as it passes through the transient temperature field. This information can be readily provided by the thermographic images.

A consequence of the above statement is that the spatial and thermal accuracy of the information is of the utmost importance and that a whole-field image is essential. This requirement means that images must be corrected for any spatial distortion and with regard to emissivity calibration.

CONCLUSIONS

1. The use of thermographic imaging in the context of open-arc MIG welding has been successfully demonstrated on a practical scale.
2. Thermal imaging provides whole-field information in a practical situation, and it therefore constitutes a unique tool for the evaluation of inputs to a thermo-mechanical determination of distortion or residual stress caused by a welding process.
3. As the thermal image provides direct evidence of transient temperatures, this approach avoids the need for complex theoretical determinations in the input stage of a thermo-mechanical computation. The theoretical approach has severe weaknesses, as material thermal properties are usually not known with certainty, and boundary conditions may also be complex in a practical situation.
4. Suitable techniques and algorithms for spatial and temperature calibration of the images, necessary for accurate prediction of outcomes, have been developed and are presented in the paper.

REFERENCES

[1] Rosenthal, D. 1946. “The Theory of Moving Sources of Heat and its Application to Metal Treatments.” *Transactions of the American Society of Mechanical Engineering* 68, no. 8: 849-66.
[2] Rykalin, N. N. 1947. *Thermal Welding Principles*. SSSR: I.A.N.
[3] Wells, A. A. 1952. “Heat Flow in Welding.” *Welding Journal* 31:263s-67s.
[4] Lindgren, L. E. 2001. “Finite Element Modeling and Simulation of Welding. Part 1: Increased Complexity.” *Journal of Thermal Stresses* 24:141-92.

[5] Lindgren, L. E. 2001. “Finite Element Modeling and Simulation of Welding. Part 2: Improved Material Modeling.” *Journal of Thermal Stresses* 24:195-231.
[6] Cheng, W., J. R. Dydo, Z. Feng, Y. Chen, and J. S. Cromptom. 2000. “Finite Element Modeling of Angular Distortion in Stiffened Thin-Section Panels.” *Proceedings of the Ninth International Conference on Computer Technology in Welding*, no.949: 120-29.
[7] Khan, M. A., N. H. Madsen, and B. A. Chin. 1984. “Infrared Thermography as a Control for the Welding Process.” *Proceedings of SPIE--The International Society for Optical Engineering* 446:154-63.
[8] Boillot, J. P., P. Ceilo, G. Begin, C. Michel, M. Lessard, P. Fafard, and D. Villemure. 1985. “Adaptive Welding by Fiber Optic Thermographic Sensing: An Analysis of Thermal and Instrumental Considerations,” *Welding Research Supplement* 64:209s-17s.
[9] Camilleri, D., T. Comlekci, C. K. Lee, H. Tan, and T. G. F. Gray. 2003. “Investigation of Temperature Transients During Flux-Cored CO_2/Ar Butt Welding of CMn Steel Plates.” *Proceedings of the International Conference on Metal Fabrication and Welding Technology (METFAB – 200*3) (September): 107-16.
[10] Friedman, E. 1975. “Thermomechanical Analysis of the Welding Process Using the Finite Element Method.” *ASME Journal of Pressure Vessel Technology* 97, no.3: 206-13.
[11] Camilleri, D., T. Comlekci, and T. G. F. Gray. 2003. “Out-of-plane Distortion of CMn Steel Plates During Flux-Cored CO_2/Ar Butt Welding.” *Proceedings of the International Conference on Metal Fabrication and Welding Technology (METFAB – 2003)* (September): 117-27.
[12] Camilleri, D., T. Comlekci, and T. G. F. Gray. (Under review.) “Computational Prediction of Out-of-Plane Welding Distortion and Experimental Investigation.” *Journal of Strain Analysis in Engineering Design*.

ACKNOWLEDGEMENTS

The financial support was provided from EPSRC grant no. GR/R335407/01. BAE SYSTEMS Marine Ltd, Govan, are thanked for welding equipment, material, and moral support.